Complex Dynamics at Conical Intersections: Vibronic Spectra and Ultrafast Decay of Electronically Excited Trifluoroacetonitrile Radical Cation

T. Mondal and S. Mahapatra*

School of Chemistry, University of Hyderabad, Hyderabad 500046, India

Received: February 7, 2008; Revised Manuscript Received: April 29, 2008

An ab initio quantum dynamical study is performed here to examine the complex nuclear motion underlying the first two photoelectron bands of trifluoroacetonitrile. The highly overlapping structures of the latter are found to originate from transitions to the five lowest electronic states (viz., $\tilde{X}^2E$, $\tilde{A}^2A_1$, $\tilde{B}^2A_2$, $\tilde{C}^2A_1$, and $\tilde{D}^2E$) of the trifluoroacetonitrile radical cation. The Jahn−Teller (JT) instability of the doubly degenerate $\tilde{X}$ and, $\tilde{D}$ and their pseudo-Jahn−Teller (PJT) interactions with the nondegenerate $\tilde{A}$, $\tilde{B}$, and $\tilde{C}$ electronic states along the degenerate vibrational modes lead to multiple multidimensional conical intersections and complex nuclear trajectories through them. It is found that the JT splitting is very weak in the $\tilde{X}$ and relatively stronger in the $\tilde{D}$ state. However, the PJT couplings play the pivotal role in the detailed shape of the vibronic bands of the radical cation. Ultrafast nonradiative decay of electronically excited radical cation has been examined. The findings of this paper are compared with the experimental data and are also discussed in relation to those observed for the methyl cyanide radical cation.

I. Introduction

Understanding the role of excited molecular electronic states is a distressing problem in contemporary chemical dynamics. Recent progress in the experimental measurements have invalidated the treatment of the electronic and nuclear motion separately within the well celebrated theoretical framework of Born−Oppenheimer (BO) approximation.[1,2] Complex pattern of molecular electronic spectra indeed bears the signature of complex entanglement of these two microscopic motions.[3] A current thrust in the theoretical treatment of chemical dynamics is to go beyond the BO picture to unravel such complex entanglement.[2,4,5] The Jahn−Teller (JT) active molecular systems fall in an unique class, in which the electron−nuclear coupling is inbuilt.[6–9] Symmetry-allowed electronic degeneracy in these systems splits upon distortions along suitable symmetry reducing nuclear vibrations. As a result, the JT split component electronic states cross at the equilibrium the geometry of the undistorted configuration and form conical intersections [2,3,10,11] of potential energy surfaces (PESs). Despite this, symmetry-allowed conical intersections of degenerate and nondegenerate electronic states or two nondegenerate electronic states are also possible.[3,9] Occurrence and ubiquity of conical intersections in molecular systems have proven the important role of electronic nonadiabatic interactions in modern chemical dynamics.[2,4,5] The trifluoroacetonitrile radical cation (CF_3CN^+) turned out to be a very challenging system, in which the electronic nonadiabatic effects seem to prevail with its highest degree of complexity. Two of its lowest vibronic bands recorded in photoelectron spectroscopy experiments[12] reveal structures that are attributed to originate from five (seven when JT effect is considered) low-lying electronic states of this species.

The equilibrium configuration of the trifluoroacetonitrile (CF_3CN) molecule belongs to the C_{3v} symmetry point group. Ionization of an electron from each of its five highest occupied $6e$, $10a_1$, $1a_2$, $9a_1$, and $5e$ molecular orbitals (MOs) yields CF_3CN^+ in its ground state $\tilde{X}^2E$ and first four excited electronic states $\tilde{A}^2A_1$, $\tilde{B}^2A_2$, $\tilde{C}^2A_1$, and $\tilde{D}^2E$. The 12 vibrational degrees of freedom of CF_3CN are grouped into $4a_1 + 4e$ irreducible representations of the C_{3v} symmetry point group. The symmetrized direct product of two E representations in this point group yields

$$(E)^2 = a_1 + e \tag{1}$$

Similarly, the direct products of $E \otimes A_1$ and $E \otimes A_2$ in the C_{3v} symmetry point group result

$$E \otimes A_1 = e \qquad E \otimes A_2 = e \tag{2}$$

These symmetry rules suggest that the degenerate $\tilde{X}^2E$ and $\tilde{D}^2E$ electronic states of CF_3CN would undergo JT splitting in first order when distorted along the degenerate vibrational modes of e symmetry (note that the symmetry of the electronic and nuclear degrees of freedom are designated by the upper and lower case symbols, respectively). From eq 2, it can be seen that the same JT active degenerate vibrational modes also cause pseudo-Jahn−Teller (PJT) type[3,13–15] of coupling between different electronic states. The totally symmetric a_1 vibrational modes, on the other hand, cannot lift the electronic degeneracy and are Condon active.[3] The impact of these four JT and PJT active degenerate and four Condon active totally symmetric vibrational modes in the vibronic dynamics of CF_3CN^+ in its five low-lying electronic states is examined below.

The photoelectron spectrum of CF_3CN has been recorded by various experimental groups by using He I, He II, and synchrotron radiation[12,16] as ionization sources. These experiments revealed different energy resolution and intensity of peaks in the vibronic bands. The first two photoelectron bands in the 13.3−17.7 eV energy range revealed highly overlapping and diffuse vibronic structures. They are attributed to the vibronic structures of the energetically close-lying five lowest electronic states of CF_3CN^+.[12,16]

Here, we attempt to develop a theoretical model in order to examine the nuclear motion underlying the vibronic structures of the mentioned photoelectron bands. It is clear from the discussion above that various electronic coupling mechanisms

* Corresponding author. E-mail: smsc@uohyd.ernet.in. Fax: +91-40-23012460.

10.1021/jp801138a CCC: $40.75
Published on Web 08/14/2008

TABLE 1: Symmetry, Frequency, and Description of the Normal Vibrational Modes of the Electronic Ground State of Trifluoroacetonitrile[a]

	vibrational frequency (ω_i)/eV				
mode	MP2/6-311++G**	experiment	predominant nature	coordinate	
			a_1		
ν_1	0.2716	0.2821	C−N stretching	Q_1	
ν_2	0.1559	0.1521	C−C stretching	Q_2	
ν_3	0.1010	0.0994	CF_3 bending	Q_3	
ν_4	0.0656	0.0647	umbrella bending	Q_4	
			e		
ν_5	0.1508	0.1505	C−F stretching	Q_{5x}	Q_{5y}
ν_6	0.0779	0.0766	C−C−F scissoring	Q_{6x}	Q_{6y}
ν_7	0.0583	0.0574	F−C−C twisting	Q_{7x}	Q_{7y}
ν_8	0.0234	0.0243	C−C−N bending + F−C−F twisting	Q_{8x}	Q_{8y}

[a] The experimental results are reproduced from ref 24. Note that theoretical frequencies are harmonic, whereas experimental ones are fundamental.

need to be incorporated in the model to reach a satisfying interpretation of the highly overlapping and complex structures of the latter. Our theoretical model consists of five low-lying (seven altogether when JT splitting is taken into consideration) electronic states of CF_3CN^+ plus its 12 vibrational degrees of freedom. The JT coupling within the $\tilde{X}$ and $\tilde{D}$ electronic states and their PJT coupling with the $\tilde{A}$, $\tilde{B}$, and $\tilde{C}$ electronic states are taken into consideration. The PJT coupling between the JT split $\tilde{X}$ and $\tilde{D}$ electronic states are not considered, mainly because they are vertically ∼3.32 eV apart and will be addressed in a future publication. Whereas the JT coupling due to e vibrational modes and the Condon activity due to a_1 vibrational modes are treated up to second order, the PJT coupling due to e vibrational modes is treated with a linear coupling scheme.

Detailed ab initio electronic structure calculations are carried out to derive the relevant coupling parameters of the vibronic Hamiltonian. A time-independent matrix diagonalization approach to treat the nuclear dynamics on seven interacting electronic states including 12 vibrational degrees of freedom is computationally impracticable. This task is therefore accomplished with a time-dependent wave packet (WP) propagation approach within the multiconfiguration time-dependent Hartree (MCTDH) scheme.[17–20] The MCTDH scheme has been very successful particularly in treating the multistate and multimode vibronic coupling problems of large dimensions. The details of the MCTDH method is documented in a recent review article by Beck et al.[20] Although the final results of this paper are obtained by this method, comparison calculations are carried out in reduced dimensions by the time-independent matrix diagonalization approach, in order to check the consistencies of various results and also identify the detailed progressions in the vibronic bands. A systematic treatment of the nuclear dynamics revealed that PJT interactions among the first five electronic states CF_3CN^+ play an important role in the nuclear dynamics. The theoretical results are found to be in excellent accord with the experimental data, revealing that the JT effect is particularly weak in the $\tilde{X}$ state. This effect is relatively stronger in the $\tilde{D}$ state. However, the PJT couplings between the $\tilde{X}-\tilde{A}$ and $\tilde{B}-\tilde{C}-\tilde{D}$ electronic states are primarily important for the highly diffuse vibronic band shapes of the radical cation.

II. Equilibrium Structure and Normal Vibrational Modes of the Electronic Ground-State of CF_3CN

The electronic structure calculations of CF_3CN are carried out at the Møller-Plesset perturbation (MP2) level of theory and by employing both cc-pVDZ as well as 6-311++g** basis sets by using Gaussian-03 program package.[21] The optimized equilibrium geometry of its electronic ground state ($\tilde{X}^1A_1$) belongs to the C_{3v} symmetry point group. The optimized geometry parameters are r_{CF} = 1.33 Å, r_{CC} = 1.48 Å, r_{CN} = 1.17 Å, ∠F−C−F = 108.54° and ∠C−C−F = 109.33°, in good agreement with their experimental values,[22] 1.33 Å, 1.49 Å, 1.15 Å, 109.23°, and 109.74° respectively. Examination of occupied canonical MOs reveals a configuration,... $(3e)^4(4e)^4(5e)^4(9a_1)^2$-$(1a_2)^2(10a_1)^2(6e)^4$ for the electronic ground state of CF_3CN. The sequence of MOs above are in agreement with the results of Shimizu et al.[22] and differs with the results of Åsbrink et al.,[23] and understandably the difference arises from the level of quantum chemistry calculations that could be performed at that time.

The highest occupied MO (HOMO) (6e), HOMO-1 (10a_1), HOMO-2 (1a_2), HOMO-3 (9a_1), and HOMO-4 (5e) are schematically shown in Figure 1 of the Supporting Information. According to Shimizu et al.,[22] the characteristics of these MOs are as follows: HOMO is C−N π bonding, HOMO-1 is mainly the nitrogen lone pair, HOMO-2 is nonbonding and purely F 2p lone-pair, and HOMO-3 is delocalized over the entire molecule and is bonding in nature. HOMO-4 is mostly F 2p lone-pair but also reveals C−F bonding. The diagrams, shown in Figure 1 of the Supporting Information, describe the nature of these MOs illustrated above. These MOs are energetically close lying. The $\tilde{A}$, $\tilde{B}$, $\tilde{C}$, and $\tilde{D}$ electronic states are vertically ∼0.50, ∼2.67, ∼2.84, and ∼3.32 eV above the $\tilde{X}$ state of CF_3CN^+. The harmonic frequencies (ω_i, i = 1−12) of the vibrational modes of the electronic ground state of CF_3CN are calculated by diagonalizing the MP2 force field and are given in Table 1 along with their fundamental values available from the experiment.[24] Along with the frequencies, the mass weighted normal coordinates are obtained, which are transformed into their dimensionless form by multiplying with $(\omega_j)^{1/2}$ (in atomic units used here).[25] These coordinates represent the normal displacement coordinates (from their equilibrium value at Q = 0), referred here as Q_i for the ith vibrational mode. The 12 vibrational modes are schematically shown in Figure 2 of the Supporting Information, and their predominant nature is given in Table 1.

III. Vibronic Coupling Model

Electronic structure and nuclear dynamics of CF_3CN^+ in its coupled $\tilde{X}-\tilde{A}-\tilde{B}-\tilde{C}-\tilde{D}$ electronic states are examined here. As mentioned above, these electronic states are energetically close and are readily accessible upon photoionization of CF_3CN and

give rise to highly overlapping vibronic bands. An analysis of the structure of the latter requires the potential energies of these electronic states and their interaction potentials along various nuclear coordinates. The two degenerate ($\tilde{X}$ and $\tilde{D}$) electronic states of CF_3CN^+ undergo a JT splitting upon displacement along the degenerate vibrational modes. The latter modes by symmetry can also cause PJT-type coupling between the two degenerate states (which is not considered here and will be addressed in a future publication) and also between the degenerate and nondegenerate electronic states. The four totally symmetric vibrational modes are Condon active within each electronic state.[3] In order to describe these couplings in the vibronic Hamiltonian, we use a diabatic electronic basis,[26,27] in which they are represented in the electronic part and are smoothly varying functions of nuclear coordinates. The Hamiltonian is written in terms of the dimensionless normal coordinates of the vibrational modes of CF_3CN as discussed above and defined in Table 1, in conjunction with the stated symmetry selection rules (eqs 1 and 2). Therefore, the Hamiltonian for the coupled manifold of seven electronic states of CF_3CN^+ can be written as

$$\mathscr{H} = \mathscr{H}_0 \mathbf{1}_7 + \begin{pmatrix} W_1^X & W_{12}^X & W_1^{X-A} & W_1^{X-B} & W_1^{X-C} & 0 & 0 \\ & W_2^X & W_2^{X-A} & W_2^{X-B} & W_2^{X-C} & 0 & 0 \\ & & W^A & 0 & 0 & W_1^{A-D} & W_2^{A-D} \\ & & & W^B & 0 & W_1^{B-D} & W_2^{B-D} \\ & h.c. & & & W^C & W_1^{C-D} & W_2^{C-D} \\ & & & & & W_1^D & W_{12}^D \\ & & & & & & W_2^D \end{pmatrix} \quad (3)$$

Here, $\mathscr{H}_0 = T_N + V_0$ represents the Hamiltonian of the unperturbed electronic ground state of CF_3CN. Nuclear motions in the latter are treated as harmonic with

$$T_N = -\frac{1}{2}\sum_{i=1}^{4}\omega_i\frac{\partial^2}{\partial Q_i^2} - \frac{1}{2}\sum_{i=5}^{8}\omega_i\left(\frac{\partial^2}{\partial Q_{ix}^2} + \frac{\partial^2}{\partial Q_{iy}^2}\right) \quad (4)$$

and

$$V_0 = \frac{1}{2}\sum_{i=1}^{4}\omega_i Q_i^2 + \frac{1}{2}\sum_{i=5}^{8}\omega_i(Q_{ix}^2 + Q_{iy}^2) \quad (5)$$

The matrix Hamiltonian with elements W in eq 3 describes the change in the electronic energy upon ionization from this unperturbed electronic ground state and defines the details of diabatic electronic PESs of CF_3CN^+.[3] These elements are expanded in a Taylor series around the equilibrium geometry of CF_3CN along each normal mode displacement coordinates. By excluding various intermode coupling terms, the following expansions are retained for these elements:

$$W_{1,2}^{X(D)} = E_0^{X(D)} + \sum_{i=1}^{4}\kappa_i^{X(D)}Q_i \pm \sum_{i=5}^{8}\lambda_i^{X(D)}Q_{ix} + \frac{1}{2}\sum_{i=1}^{4}\gamma_i^{X(D)}Q_i^2 + \frac{1}{2}\sum_{i=5}^{8}[\gamma_i^{X(D)}(Q_{ix}^2 + Q_{iy}^2) \pm \eta_i^{X(D)}(Q_{ix}^2 - Q_{iy}^2)] + \frac{1}{6}\sum_{i=5}^{8}[\delta_i^{X(D)}(-6Q_{ix}Q_{iy}^2 + 2Q_{ix}^3) \pm \mu_i^{X(D)}(Q_{ix}^3 + Q_{ix}Q_{iy}^2)] + \frac{1}{24}\sum_{i=5}^{8}[\zeta_i^{X(D)}(Q_{ix}^2 + Q_{iy}^2)2 \pm \alpha_i^{X(D)}(Q_{ix}^4 - 6Q_{ix}^2Q_{iy}^2 + Q_{iy}^4) \pm \beta_i^{X(D)}(Q_{ix}^4 - Q_{iy}^4)] \quad (6a)$$

$$W_{12}^{X(D)} = \sum_{i=5}^{8}\lambda_i^{X(D)}Q_{iy} - \sum_{i=5}^{8}\eta_i^{X(D)}Q_{ix}Q_{iy} + \frac{1}{6}\sum_{i=5}^{8}\mu_i^{X(D)}(Q_{ix}^2Q_{iy} + Q_{iy}^3) + \frac{1}{24}\sum_{i=5}^{8}[4\alpha_i^{X(D)}Q_{ix}Q_{iy}(Q_{ix}^2 - Q_{iy}^2) - 2\beta_i^{X(D)}Q_{ix}Q_{iy}(Q_{ix}^2 + Q_{iy}^2)] \quad (6b)$$

$$W_1^{X(D)-k} = \sum_{i=5}^{8}\lambda_i^{X(D)-k}Q_{ix} \quad (6c)$$

$$W_2^{X(D)-k} = -\sum_{i=5}^{8}\lambda_i^{X(D)-k}Q_{iy} \quad (6d)$$

$$W^k = E_0^k + \sum_{i=1}^{4}\kappa_i^kQ_i + \frac{1}{2}\sum_{i=1}^{4}\gamma_i^kQ_i^2 + \frac{1}{2}\sum_{i=5}^{8}\gamma_i^k(Q_{ix}^2 + Q_{iy}^2) + \frac{1}{24}\sum_{i=5}^{8}\zeta_i^k(Q_{ix}^4 + Q_{iy}^4) \qquad k \in \tilde{A}, \tilde{B}, \text{ and } \tilde{C} \quad (6e)$$

The quantity E_0^j represents the vertical ionization potential of the jth electronic state. The linear intrastate and JT coupling parameters of the jth electronic state are denoted by κ_i^j and λ_i^j for the symmetric and degenerate vibrational modes, respectively. The linear PJT coupling parameters for the latter modes between the electronic states j and k are represented by λ_i^{j-k}. The diagonal second-order coupling parameters for the vibrational modes are given by γ_i^j, and η_i^j represents the quadratic JT coupling parameters for the degenerate vibrational modes. The diagonal cubic and quartic[28] coupling parameters for these vibrational modes are given by δ_i^j and ζ_i^j, whereas the corresponding off-diagonal coupling parameters are given by μ_i^j, α_i^j, and β_i^j. To calculate these coupling parameters, we perform direct calculations of vertical ionization energies (VIEs) of CF_3CN by the outer valence Green's function method[29] by employing the same basis sets as the one noted above. The VIEs are calculated for $Q_i = \pm 0.10, \pm 0.25$ (0.25), $\pm$ 1.50, along the ith vibrational mode, keeping others at their equilibrium value. These VIEs are equated with the adiabatic potential energies of CF_3CN^+ relative to the electronic ground state of CF_3CN. Subsequently, these energies are fitted to the adiabatic form of the diabatic electronic Hamiltonian of eq 3 by using least-squares algorithm, and thereby, the coupling parameters are obtained. Because the latter represent the derivatives of various order in the Taylor series expansion of the elements of the electronic Hamiltonian of (eqs 6a and 6e), they are also estimated by numerical finite difference schemes. The parameters that represent the best agreement between the model and the ab initio adiabatic potentials are given in Tables 2, 3, and 4.

IV. Dynamical Observables

The dynamical observables are reported in terms of vibronic spectra and nonradiative decay of excited electronic states. The spectral intensity, $P(E)$, of the vibronic band is calculated by the Fermi's golden rule equation:

$$P(E) = \sum_v |\langle\Psi_v^f|\hat{T}|\Psi_0^i\rangle|^2\delta(E - E_v^f + E_0^i) \quad (7)$$

Here, $|\Psi_v^f\rangle$ represents the eigenstates of the vibronic Hamiltonian of eq 3 with energy E_v^f. $|\Psi_0^i\rangle$ is the initial ground vibronic state of neutral CF_3CN with energy E_0^i. The quantity $\hat{T}$ is the operator that describes the interaction of valence electrons with the external radiation. The quantity E is the difference of energy

of the external radiation and the kinetic energy of the ejected electron and therefore represents the electron binding energy or the ionization energy. The initial vibronic state is assumed to take the form

$$|\Psi_0^i\rangle = |\Phi_0\rangle\,|\chi_0^0\rangle \tag{8}$$

with $|\Phi\rangle$ and $|\chi\rangle$ representing the diabatic electronic and vibrational components of the wave function, respectively. The latter are taken to be the eigenfunction of the unperturbed harmonic Hamiltonian, $\mathscr{H}_0$ (cf., eqs 4 and 5).

In a time-dependent picture, eq 7 for the spectral intensity rearranges to a Fourier transform of the time autocorrelation function of the WP[27]

$$P(E) \approx 2\mathrm{Re}\int_0^\infty e^{iEt/\hbar}\langle 0|\tau^\dagger\, e^{-iHt/\hbar}\,\tau|0\rangle\, dt \tag{9}$$

$$\approx 2\mathrm{Re}\int_0^\infty e^{iEt/\hbar} C^m(t)\, dt \tag{10}$$

The quantity, $C^m(t) = \langle\Psi^m(0)|\Psi^m(t)\rangle$, is the time autocorrelation function of the WP initially prepared on mth electronic state. τ refers to the transition dipole matrix; $\tau^\dagger = (\tau^{\tilde{X}_x}, \tau^{\tilde{X}_y}, \tau^{\tilde{A}}, \tau^{\tilde{B}}, \tau^{\tilde{C}}, \tau^{\tilde{D}_x}, \tau^{\tilde{D}_y})$, with, $\tau^m = \langle\psi^m|\hat{T}|\psi^0\rangle$. Note that the final wave function possesses components on each of the vibronically coupled seven diabatic electronic states ($\tilde{X}_x$, $\tilde{X}_y$, $\tilde{A}$, $\tilde{B}$, $\tilde{C}$, $\tilde{D}_x$, and $\tilde{D}_y$), and therefore, the composite vibronic spectrum is to be written as a weighted sum of the resulting seven partial spectra. The latter are calculated by propagating WPs for seven different initial conditions. The diabatic electronic populations are calculated by following the change in the probability density ($|\psi|^2$) of the WP component on each electronic state in time. This yields informations on the nonradiative decay of the excited electronic states of CF_3CN^+.

V. Numerical Computations

The vibronic eigenvalue spectrum of the matrix Hamiltonian $\mathscr{H}$ of eq 3 can be calculated either by a time-independent matrix diagonalization or a time-dependent WP method. In the former approach, the eigenvalue equation, $\mathscr{H}|\Psi_v\rangle = E_v|\Psi_v\rangle$, is solved by representing $\mathscr{H}$ in a complete direct product basis of diabatic electronic states Φ^m and one-dimensional harmonic oscillator eigenfunctions, $|v_i\rangle$ ($i = 1-12$), of $\mathscr{H}_0$. The vibronic Hamiltonian expressed in this basis becomes a function of the occupation number of various vibrational modes.[3] The maximum level of excitation for each mode is approximately estimated from its excitation strength[3]

TABLE 2: Parameters of the Vibronic Hamiltonian for the Degenerate $\tilde{X}^2E$ Electronic State of CF_3CN^+, Derived from the Ab Initio Electronic Structure Results (See Text for Details)[a]

mode	κ_i or λ_i	γ_i	η_i	ζ_i	ϕ_i	μ_i	α_i	β_i
ν_1	0.2779	0.0325						
ν_2	0.2890	−0.0165						
ν_3	−0.0669	0.0005						
ν_4	−0.0040	−0.0027						
ν_5	0.0109	−0.0100	−0.0032	−0.0080	−0.0060	−0.0008	−0.0003	−0.0002
ν_6	0.0082	−0.0070	0.0037	−0.0040	−0.0025	0.0009	0.0005	0.0002
ν_7	0.0093	−0.0085	−0.0013	−0.0063	−0.0040	0.0009	0.0004	0.0002
ν_8	0.0092	−0.0082	−0.0004	−0.0065	−0.0061	−0.0003	−0.0002	−0.0002
E_0^X	14.031							

[a] The VIE of this electronic state (E_0^X) is also given in the table. All quantities are in eV.

TABLE 3: Parameters of the Vibronic Hamiltonian for the Three Lowest Nondegenerate $\tilde{A}^2A_1$, $\tilde{B}^2A_2$, and $\tilde{C}^2A_1$ Electronic States of CF_3CN^+, Derived from the Ab Initio Electronic Structure Results (See Text for Details)[a]

mode	κ_i $\tilde{A}/\tilde{B}/\tilde{C}$	γ_i $\tilde{A}/\tilde{B}/\tilde{C}$	ϕ_i $\tilde{A}/\tilde{B}/\tilde{C}$
ν_1	−0.0927/0.0515/−0.0915	−0.0081/−0.0033/−0.0163	
ν_2	0.2612/−0.1642/0.1685	−0.0271/−0.0110/−0.0229	
ν_3	−0.0326/0.0593/−0.0639	−0.0003/−0.0107/ 0.0065	
ν_4	0.0270/−0.0744/0.0907	−0.0006/ 0.0029/−0.0039	
ν_5		−0.0075/−0.0916/−0.0514	−0.0020/−0.0002/−0.0007
ν_6		−0.0037/−0.0182/−0.0184	−0.0025/−0.0030/−0.0050
ν_7		0.0022/−0.0280/−0.0077	0.0009/−0.0035/−0.0029
ν_8		0.0066/−0.0048/−0.0080	0.0019/−0.0015/−0.0035
E_0^A	14.529		
E_0^B	16.701		
E_0^C	16.872		

[a] The VIEs of these three electronic states (E_0^A, E_0^B, E_0^C) are also given in the table. All quantities are in eV.

TABLE 4: Same as in Table 2 for the Degenerate $\tilde{D}^2E$ Electronic State of CF_3CN^+

mode	κ_i or λ_i	γ_i	η_i	ζ_i	ϕ_i	μ_i	α_i	β_i
ν_1	0.0556	0.0033						
ν_2	−0.2526	0.0037						
ν_3	0.0231	−0.0098						
ν_4	−0.0945	−0.0075						
ν_5	0.1910	−0.0348	−0.0742	−0.0008	−0.0008	−0.0006	−0.0005	−0.0003
ν_6	0.0428	0.0023	−0.0044	0.0009	0.0005	−0.0009	−0.0005	−0.0003
ν_7	0.0614	−0.0026	−0.0020	−0.0006	−0.0004	−0.0007	−0.0004	−0.0002
ν_8	0.0014	−0.0010	0.0008	0.0007	0.0005	0.0005	0.0004	0.0001
E_0^D	17.350							

$$\left[\frac{1}{2}\left(\frac{\kappa \text{ or } \lambda}{\omega}\right)^2\right]$$

One usually obtains a highly sparse Hamiltonian matrix in such a direct product basis. It is then tridiagonalized by using the Lanczos algorithm prior to diagonalization.[30] The diagonal elements of the resulting eigenvalue matrix give the energies of the vibronic energy levels, and the relative intensities of the vibronic lines are calculated from the squared first components of the Lanczos eigenvectors.[31]

In the time-dependent approach, a suitable WP is propagated in the final electronic state by solving the eigenvalue equation, $i\hbar\partial_t|\Psi_v\rangle = \mathscr{H}|\Psi_v\rangle$. The autocorrelation function, $C^m(t)$, of the WP is recorded in time and Fourier transformed to generate the vibronic eigenvalue spectrum. The time-independent matrix diagonalization approach often becomes unsuitable for multistate and multimode problems (such as the present example) because of very large computer hardware requirements. The WP propagation within the MCTDH scheme has emerged as a very promising alternative tool to deal with such situations.[17–20] The efficiency of this algorithm lies in its multiset ansatz, which allows a combination of several vibrational degrees of freedom to effectively reduce the dimensionality problem. By applying this ansatz, the wave function for the present nonadiabatic problem can be expressed as[20]

$$\Psi(Q_1, Q_2, ..., Q_f, t) = \Psi(q_1, q_2, ..., q_p, t)$$

$$= \sum_{\alpha=1}^{7} \sum_{j_1=1}^{n_1^{(\alpha)}} ... \sum_{j_p=1}^{n_p^{(\alpha)}} A_{j_1...j_p}^{(\alpha)}(t) \prod_{k=1}^{p} \phi_{j_k}^{(\alpha,k)}(q_k, t)|\alpha\rangle \quad (11)$$

$$= \sum_{\alpha} \sum_{J} A_J^{(\alpha)} \Phi_J^{(\alpha)}|\alpha\rangle \quad (12)$$

where f and p represent the number of vibrational degrees of freedom and particles defining combined vibrational modes, respectively. $A_{j_1...j_p}^{(\alpha)}$ denote the MCTDH expansion coefficients, and $\{\phi_{jk}^{(\alpha,k)}\}$ are the one-dimensional expansion functions, known as single particle functions (SPFs). The labels $\{\alpha\}$ are indices denoting the discrete set of electronic states considered in the calculation. Thus, the WP, $\Psi^{(\alpha)}$ $(= \sum_J A_J^{(\alpha)} \Phi_J^{(\alpha)})$, associated with each electronic state is described by using a different set of SPFs, $\{\phi_{jk}^{(\alpha,k)}\}$. Here the multi-index, $J = j_1...j_p$ depends implicitly on the state α because the maximum number of SPFs may differ for different states. The summation $\sum_J$ is a shorthand notation for summation over all possible index combinations for the relevant electronic state. The variables for the p sets of SPFs are defined in terms of one or multidimensional coordinates of a particle. The operational principles of the MCTDH algorithm are discussed in detail in the literature,[20] and we do not reiterate them here.

To solve the time-dependent Schrödinger equation by employing the MCTDH algorithm, one needs to choose a set of harmonic oscillator discrete variable representation function, as a primitive basis. The SPFs, their time derivatives, and the Hamiltonian are then represented in this basis at each point in time.[20] A combination scheme for the twelve vibrational degrees of freedom of CF_3CN is then set up to reduce the computational requirements, and finally, a set of SPFs is specified in order to accurately represent the evolving WP. The initial SPFs used are sets of ortho-normalized harmonic oscillator functions in the mass-frequency scaled coordinates used. In the multiset formalism, one set is required for each particle for each electronic state.[20] The initial wave function is the vibrational wave function of CF_3CN of its ground electronic state, which is simply expressed as a product of the first SPFs in each set and assumes the form of a Gaussian WP. The various mode combination schemes, the sizes of the primitive, and SPF bases used in the present calculations are given in Table 1 of the Supporting Information.

VI. Adiabatic PESs

The adiabatic PESs of the lowest five electronic states are obtained by diagonalizing the diabatic electronic Hamiltonian matrix given in eqs 3–6 by using the parameters of Tables 2, 3, and 4. One-dimensional cuts of these multidimensional PESs along the dimensionless normal coordinate of each vibrational mode are shown in Figures 1 and 2. In each plot, the points represent the adiabatic potential energies computed ab initio, and the curves superimposed on them represent those obtained by the present vibronic model of Section III. In Figure 1a−d, the potential energies of $\tilde{X}$, $\tilde{A}$, $\tilde{B}$, $\tilde{C}$, and $\tilde{D}$ electronic states (indicated in the panel) are plotted along the symmetric vibrational modes $\nu_1-\nu_4$, respectively. It can be seen that the model reproduces ab initio data extremely well. The degeneracy of the $\tilde{X}$ and $\tilde{D}$ states remains unperturbed on distortion along these symmetric vibrational modes. Although the crossing of the $\tilde{X}$ state with the others seems not very important (except with the $\tilde{A}$ state; panel a), the crossings of the $\tilde{D}$ state with $\tilde{B}$ and $\tilde{C}$ electronic states appear to have crucial role in shaping up the details structure of the second vibronic band. The participating electronic states in the latter are energetically close, and the curve crossings seen in the diagram would lead to multiple low-lying energetically accessible conical intersections among them. The locus of degeneracy of the two components of the $\tilde{X}$ and also $\tilde{D}$ electronic states define the seam of the JT conical intersections within these states, occurring at the C_{3v} symmetry configuration of CF_3CN^+. In a second-order coupling approach, the energetic minimum of these seams are given by

$$V_{\min,X(D)}^{(c)} = E_0^{X(D)} - \frac{1}{2}\sum_{i=1}^{4} \frac{(\kappa_i^{X(D)})^2}{(\omega_i + \gamma_i^{X(D)})} \quad (13)$$

With the parameters of Tables 2–4, these minima occur at, $V_{\min,X}^{(c)} \approx 13.58$ eV and $V_{\min,D}^{(c)} \approx 17.06$ eV.

The electronic degeneracy of the $\tilde{X}$ and $\tilde{D}$ states is split on distortion along the degenerate vibrational modes $\nu_5-\nu_8$, and this splitting leads to a total of seven states altogether in the $\tilde{X}-\tilde{A}-\tilde{B}-\tilde{C}-\tilde{D}$ electronic manifold. The potential energies of the $\tilde{X}$, $\tilde{A}$, $\tilde{B}$, $\tilde{C}$, and $\tilde{D}$ electronic states of CF_3CN^+ are shown in Figure 2a−d along the x component of the degenerate vibrational modes $\nu_5-\nu_8$, respectively. The symmetry rule forbids the first-order coupling due to these vibrational modes in the nondegenerate $\tilde{A}$, $\tilde{B}$, and $\tilde{C}$ electronic states. However, these modes are JT active in first order in the $\tilde{X}$ and $\tilde{D}$ states. It can be seen from Figure 2 that the JT splitting is very small in the $\tilde{X}$ state along all the degenerate vibrational modes; in contrast, significant splitting can be observed along ν_5, ν_6, and ν_7 vibrational modes in the $\tilde{D}$ state. As before, the points on the diagram are the computed adiabatic energies, and the curves superimposed on them represent the fit to the present theoretical model. Moreover, the quartic terms of the Taylor expansion (eqs 6a–6e) seem to have a significant role in representing the potential energies of the $\tilde{X}$ state, particularly along the vibrational mode ν_8. The seams of JT conical intersections in the $\tilde{X}$ and $\tilde{D}$ electronic states occur in the coordinate space of a_1 vibrational modes. The energetic minimum of these seams becomes critical point on the surface upon JT distortion. New minimum on the lower adiabatic sheets of the JT split $\tilde{X}$ and $\tilde{D}$ elecronic states occurs at ~13.57 and ~16.58 eV, respectively. Therefore, the

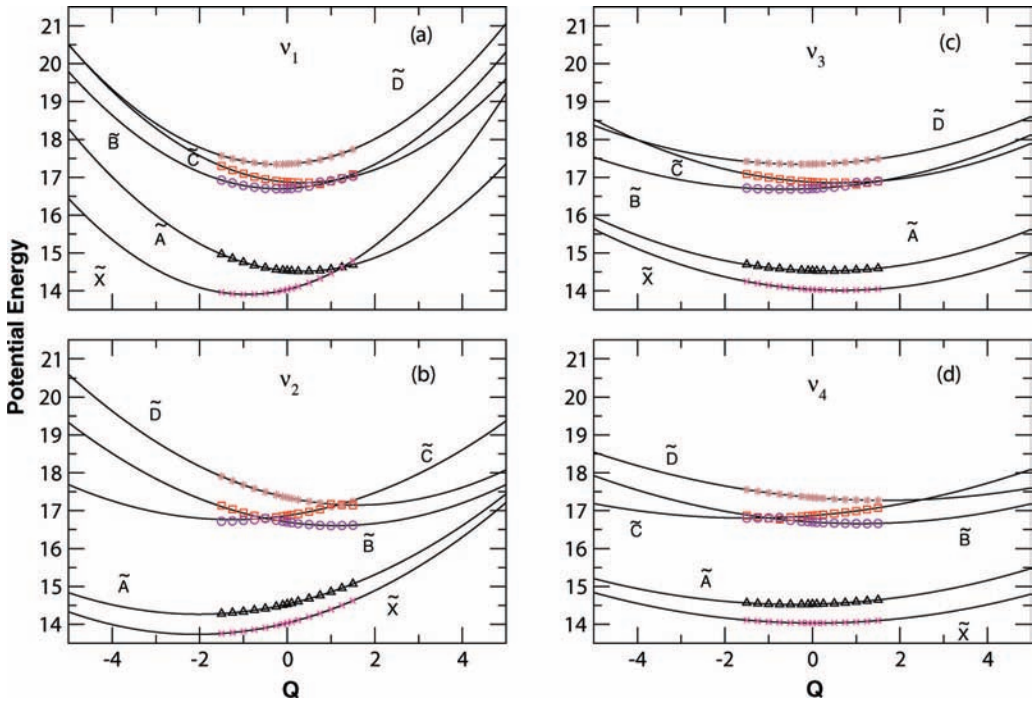

Figure 1. Adiabatic potential energies of the lowest five electronic states of CF_3CN^+ along the dimensionless normal coordinates of its four totally symmetric vibrational modes $\nu_1-\nu_4$. The potential energies obtained from the present vibronic model are shown by solid lines, and the computed ab initio data, superimposed on them, are shown by the points.

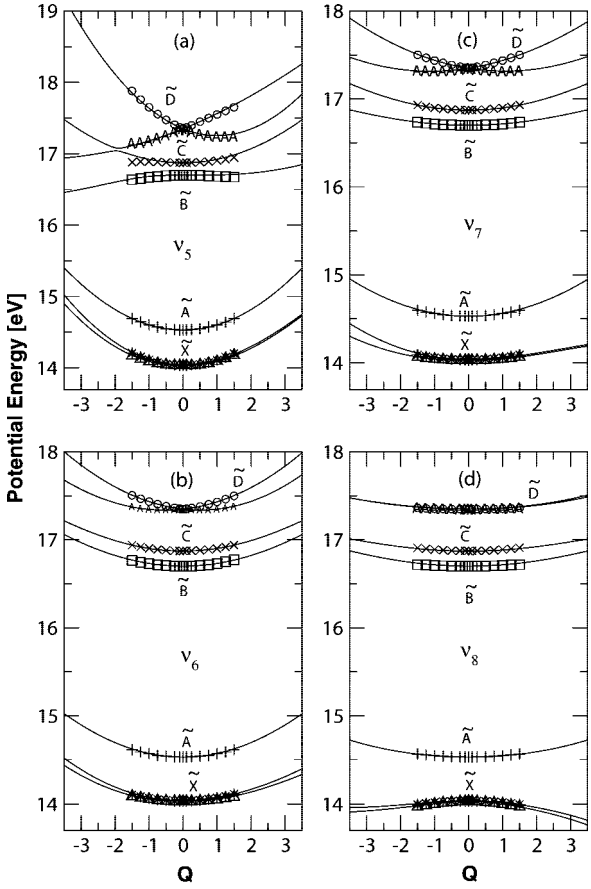

Figure 2. Same as in Figure 1, along the dimensionless normal coordinates of the x component of the degenerate vibrational modes $\nu_5-\nu_8$.

JT stabilization energies amount to $\sim 4.6 \times 10^{-3}$ and ~ 0.48 eV for the $\tilde{X}$ and $\tilde{D}$ states, respectively.

Approximate estimates of the energetic minimum of various PJT crossing seams are as follows. The minimum of the seam of $\tilde{X}-\tilde{A}$ conical intersections occurs ~ 0.43 eV above the minimum of the JT conical intersections in the $\tilde{X}$ state. The minimum of the $\tilde{X}-\tilde{B}$ and $\tilde{X}-\tilde{C}$ conical intersections occurs ~ 2.02 and ~ 1.81 eV above the latter, respectively. The minimum of the $\tilde{D}-\tilde{A}$, $\tilde{D}-\tilde{B}$, and $\tilde{D}-\tilde{C}$ conical intersections, on the other hand, occurs at ~ 0.5 and ~ 0.27 eV below and ~ 0.04 eV above the minimum of the JT conical intersections in the $\tilde{D}$ state, respectively. All these critical points of the PESs occur well within the energy range of the first two photoelectron bands studied here.

VII. Vibronic Energy Levels

Vibronic energy levels of the $\tilde{X}^2E$, $\tilde{A}^2A_1$, $\tilde{B}^2A_2$, $\tilde{C}^2A_1$, and $\tilde{D}^2E$ electronic states of CF_3CN^+ are shown and discussed in this section. These are calculated by the quantum mechanical methods described above by using the parameters of Tables 2–4. To start with, let us first examine the energy levels of each of these electronic states by excluding the PJT coupling with their neighbors and using a second-order model Hamiltonian. The final theoretical results of this paper are, however, obtained by including all couplings as described in the Hamiltonian of eq 3) and propagating WPs by using the MCTDH algorithm.[17–20] In the following, we start with various reduced dimensional models and systematical approach to carry out the final simulation of nuclear dynamics by using the seven electronic states and 12 vibrational modes.

In the uncoupled states situation and in the absence of any intermode coupling terms, the Hamiltonian for the $\tilde{X}$ and $\tilde{D}$ states are separable in terms of the a_1 and e vibrational modes. One can therefore calculate partial spectra separately for the a_1 and e vibrational modes and convolute them to generate the complete spectrum, for these degenerate electronic states. Such a separation reduces the dimension of the secular matrix and facilitates the numerical computation. The vibronic energy level spectrum

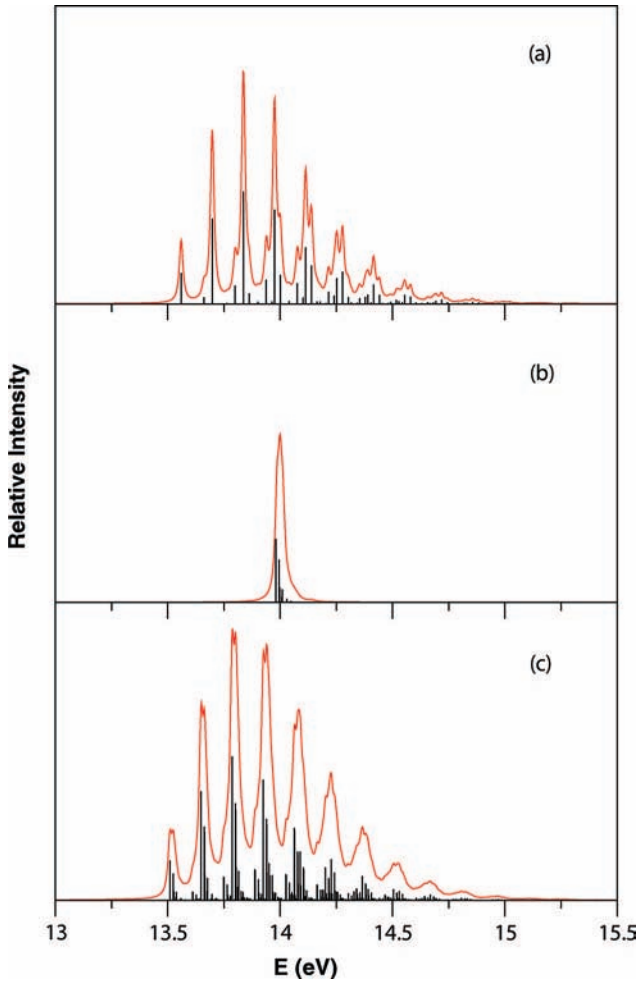

Figure 3. Vibronic energy levels of the $\tilde{X}^2E$ electronic manifold of CF_3CN^+: (a) partial spectrum computed with the four totally symmetric a_1 vibrational modes $\nu_1-\nu_4$, (b) partial spectrum computed with the four JT active degenerate e vibrational modes $\nu_5-\nu_8$, and (c) composite theoretical spectrum obtained by convoluting the above partial spectra. The relative intensity (in arbitrary units) is plotted as a function of the energy of the final vibronic state. The zero of energy corresponds to the equilibrium minimum of the electronic ground state of CF_3CN. The theoretical stick spectrum in each panel is convoluted with a Lorentzian function of 20 meV fwhm to generate the spectral envelope. The stick spectrum of panel c is multiplied by a factor of 3 for a better clarity.

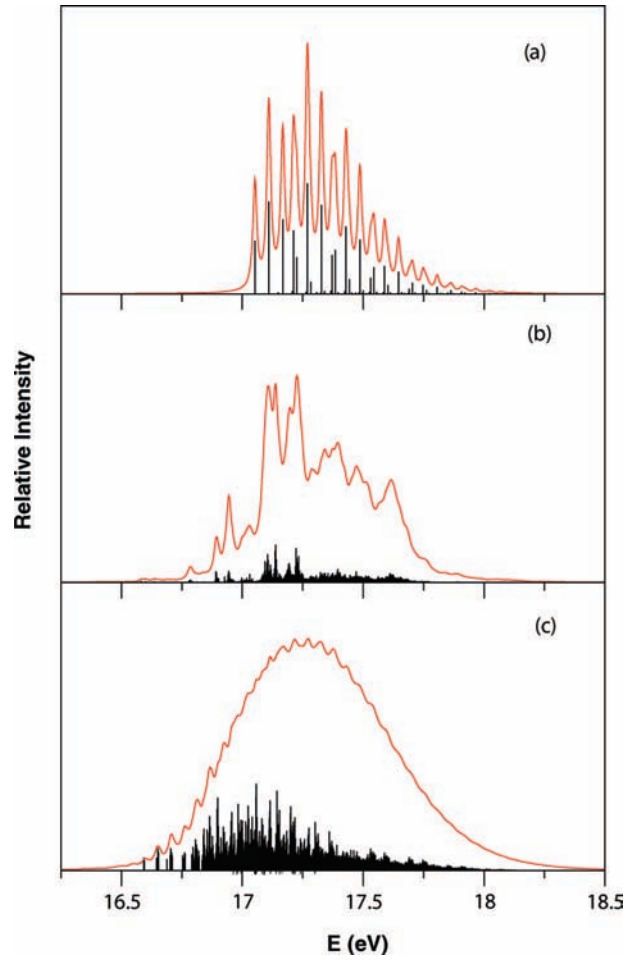

Figure 4. Same as Figure 3, $\tilde{D}^2E$ for the electronic manifold of CF_3CN^+.

of the $\tilde{X}$ electronic manifold is shown in Figure 3. The two partial spectra of the a_1 and e vibrational modes are shown in panels a and b, respectively. The results of convolution of the two partial spectra are shown in panel c. The vibronic energy eigenvalues are obtained by diagonalizing the Hamiltonian matrix by using the Lanczos algorithm and are shown as the stick lines in the figure. The envelopes are obtained by convoluting these stick lines with a Lorentzian function with a full width at the half-maximum (fwhm) of 20 meV. Further details of the calculations are given in Table 1 of the Supporting Information. The partial spectrum of the e vibrational modes (panel b) is essentially structureless because of their very weak JT coupling in the state (cf., Table 2 and Figure 2). The a_1 vibrational modes (panel a), ν_1, ν_2, and ν_3 form progressions, and peaks are ~0.302, ~0.138, and ~ 0.101 eV spaced in energy corresponding to the vibrational frequencies of these modes (cf., Table 1), respectively. The vibrational mode ν_2 forms the dominant progression in the band. Fundamental transition due to ν_7 and ν_8 vibrational modes are observed in the partial spectrum for the degenerate vibrational modes (panel b). Lines are ~0.049 and ~0.015 eV spaced in energy and correspond to the frequency of the ν_7 and ν_8 vibrational modes, respectively. Similar spectra for the JT split $\tilde{D}^2E$ electronic manifold of CF_3CN^+ are shown in Figure 4a−c. In contrast to the $\tilde{X}$ state spectrum (cf. Figure 3a), the symmetric mode spectrum for this state (panel a) reveals dominant excitations of the ν_2 and ν_4 vibrational modes. The dominant lines are ~0.058 and ~0.154 eV spaced relative to the band origin and correspond to the frequency of the ν_4 and ν_2 vibrational modes in the $\tilde{D}$ electronic state, respectively. The excitation of the ν_1 and ν_3 vibrational modes in this case are found to be much weaker compared to that in the $\tilde{X}$ state. The spectrum for the JT active vibrational modes (panel b) clearly reveals that the JT effect is much stronger in this electronic manifold. Excitations due to the degenerate ν_5, ν_6, and ν_7 vibrational modes can be found in this case. The irregular spacings of lines in the spectrum result from the multimode JT interactions. The composite vibronic spectrum shown in panel c turned out to be very diffuse because of much increase in the spectral line density arising from relatively stronger JT coupling due to the degenerate vibrational modes in the $\tilde{D}$ state.

The three nondegenerate electronic states ($\tilde{A}$, $\tilde{B}$, and $\tilde{C}$) of CF_3CN^+ lie (vertically) in between the two degenerate electronic states ($\tilde{X}$ and $\tilde{D}$). The vibronic band structures of the latter electronic states shown above in Figures 3 and 4 differ significantly from the experimental results (presented later in Figure 6). Therefore, it seems necessary to consider their possible PJT interactions with these three nondegenerate

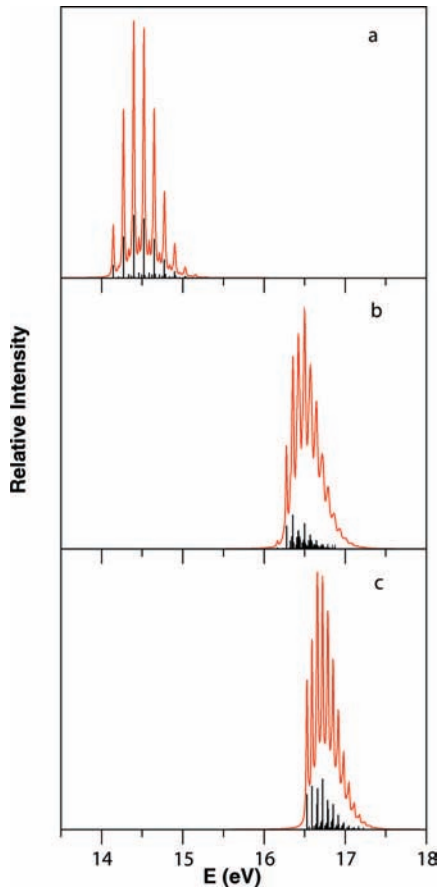

Figure 5. Same as Figure 3, for the nondegenerate $\tilde{A}^2A_1$(panel a), $\tilde{B}^2A_2$ (panel b), and $\tilde{C}^2A_1$ (panel c) electronic states of CF_3CN^+.

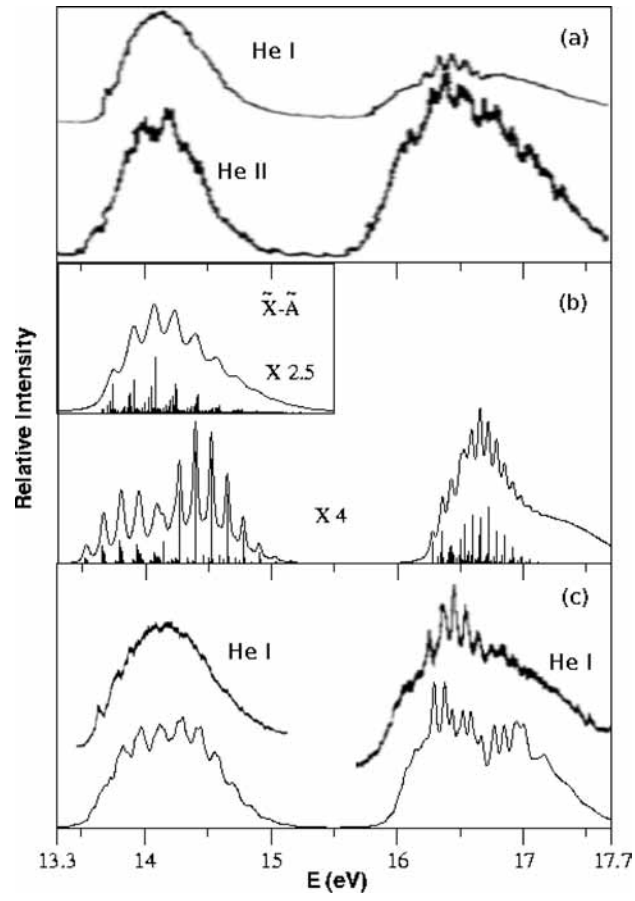

Figure 6. Comparison of the present theoretical and experimental photoelectron bands of CF_3CN: (a) He I and He II experimental spectrum,[12] (b) composite theoretical spectrum employing a full second-order Hamiltonian and without considering the PJT coupling (the stick vibronic spectrum is multiplied by a factor 4 for clear representation), and (c) final theoretical results obtained by including all couplings described in the Hamiltonian of eqs 3–6e. The theoretical spectral envelopes in panels b and c correspond to a Lorentzian line shape function with 40 meV fwhm. The vibronic stick eigenvalue spectrum obtained by diagonalizing the $\tilde{X}^2E-\tilde{A}^2A_1$ block of the Hamiltonian is shown in the inset of panel b (see text for details). The spectral envelop in it corresponds to a Lorentzian function with 40 meV fwhm. The stick vibronic spectrum is multiplied by a factor of 2.5. The magnified version of the experimental He I band is also included on top of the theoretical results of panel c for a better clarity.

electronic states to account for the detail fine structure of the first two photoelectron bands of CF_3CN. The vibronic energy level spectrum of these nondegenerate electronic states without including the coupling with their neighbors are shown in Figure 5a−c. The vibronic structure of the uncoupled $\tilde{A}^2A_1$ electronic state (panel a) reveals dominant excitation of the ν_2 vibrational mode up to its seventh overtone. The other three symmetric vibrational modes are very weakly excited in this band. The vibronic structure of the $\tilde{B}^2A_2$ (panel b) and $\tilde{C}^2A_1$ (panel c) electronic states, on the other hand, reveals dominant excitations of ν_2 and ν_4 vibrational modes. Relatively diffuse structure of the band in panel b compared to that in panel a and c is caused by the relatively large second order coupling of the degenerate vibrational modes in the $\tilde{B}$ sate (cf. Table 3).

So far, we did not consider the PJT coupling of various electronic states in the numerical calculations. On inclusion of this coupling, the separation of the Hamiltonian in terms of the symmetric and degenerate vibrational modes for the degenerate electronic states as explored above is no longer possible. It is therefore necessary to follow the nuclear dynamics simultaneously on seven coupled electronic states (four from the two JT split $\tilde{X}$ and $\tilde{D}$ states plus three nondegenerate $\tilde{A}$, $\tilde{B}$, and $\tilde{C}$ electronic states) including all relevant vibrational degrees of freedom. Computationally, it turns out to be a daunting task to simulate the nuclear dynamics quantum mechanically by the matrix diagonalization approach employed above. We therefore resort to the promising MCTDH algorithm[17–20] and propagate WPs on seven coupled electronic states including all 12 vibrational degrees of freedom in order to arrive at our goal. The 12 vibrational degrees of freedom are grouped into four three-dimensional particles. The combination scheme of the vibrational modes is given in Table 2 of the Supporting Information, along with the sizes of the primitive and SPF bases. The parameters documented there are optimally chosen to ensure the numerical convergence of the vibronic bands shown below. The WP in each calculation is propagated for 200 fs which effectively yields results for 400 fs propagation.[32]

Figure 6 displays in comparison the experimental and presents theoretical photoelectron bands of CF_3CN in the energy range 13−18 eV, resulting from ionization from the five valence type MOs of CF_3CN (cf. Figure 1 of the Supporting Information). The theoretical results are shown in panels b and c along with the experimental He I and He II results in panel a.[12] The theoretical results of panel b are obtained by superimposing the spectra shown in Figures (3–5) without considering the PJT interactions among the states. The results shown in panel c are obtained by including all coupling terms as given in the Hamiltonian of eqs 3–6 and propagating WPs by employing the MCTDH scheme.[17–20] Details of the MCTDH calculations are given in Table 2 of the Supporting Information. Seven WP propagations in the coupled $\tilde{X}-\tilde{A}-\tilde{B}-\tilde{C}-\tilde{D}$ electronic manifold

are carried out by initially preparing the WP separately on each of the component state of this manifold. Finally, results from these seven calculations are combined with appropriate statistical weights. The resulting time autocorrelation function is damped with a relaxation time of 33 fs (which corresponds to a 40 meV fwhm Lorentzian function) before Fourier transformation to generate the spectral envelopes of panel c. The stick spectrum of panel b is also convoluted with a 40 meV fwhm Lorentzian function to obtain the corresponding spectral envelope. A comparison of the theoretical results of panels b and c with the experimental one in panel a immediately reveals the strong impact of PJT interactions in the fine structure of the vibronic bands. For clarity, the experimental He I bands in magnified form are included on top of the theoretical bands of panel c. The JT couplings within the $\tilde{X}$ state and its PJT coupling with the $\tilde{A}$ state primarily contribute to the vibronic structure of the first band. The JT coupling within the $\tilde{D}$ state plus the $\tilde{B}-\tilde{C}-\tilde{D}$ PJT couplings, on the other hand, yields the irregular and highly overlapping structure of the second band. The theoretical results of panel c are in good accord with the experimental, particularly with the He II, data.

The foregoing discussions reveal that in practice, the seven coupled electronic states Hamiltonian assumes a block diagonal structure; hence, the final results can be obtained by solving the eigenvalue equations separately for each block. These blocks consist of $\tilde{X}-\tilde{A}$ and $\tilde{B}-\tilde{C}-\tilde{D}$ coupled electronic states. We attempted to diagonalize each of these two blocks of the Hamiltonian matrix separately. Although a nearly converged stick eigenvalue spectrum could be obtained for the $\tilde{X}-\tilde{A}$ block, we miserably failed (because of large computer hardware requirements) to get a presentable structure of the vibronic eigenvalue spectrum for the $\tilde{B}-\tilde{C}-\tilde{D}$ block. The nearly converged vibronic level spectrum of the $\tilde{X}-\tilde{A}$ coupled electronic states is included as an inset in panel b of Figure 6. The precise location of the adiabatic ionization positions of the seven states of CF_3CN^+ are not reported in the experimental investigations.[12] However, the onset of the experimental band is found at ~13.6 eV; we adjusted our theoretical result of the band origin to the latter value. It was necessary to decrease the VIE of the $\tilde{X}$ state by ~0.2 eV (from its ab initio value reported in Table 3) to obtain the experimentally observed maximum of the $\tilde{X}-\tilde{A}$ band at ~14.3 eV. We note that apart from this, no other adjustments of parameters (reported in various tables in this paper) are made. Precise quantitative information on the vibronic energy levels could not be extracted from the poorly resolved experimental spectra;[12,16] however, our estimates show that the dominant progressions in the $\tilde{X}-\tilde{A}$ band is caused by the vibrational mode ν_2: the peaks are ~0.144 eV apart compared to the experimental (rough) estimate of ~0.136 eV. Similarly, the dominant progression in the $\tilde{B}-\tilde{C}-\tilde{D}$ electronic states caused by the vibrational mode ν_2 and the peaks are ~0.154 eV apart compared to the estimated experimental value of ~0.140 eV.

To this end, it is worthwhile to discuss the above results in relation to those found for CH_3CN^+.[33] Substitution of F atom results into the appearance of many energetically close-lying electronic states arising from ionization from MOs of CF_3CN with predominant F lone-pair orbital character. The nature of HOMO and HOMO-1 of both CH_3CN[33] and CF_3CN is similar, describing predominantly C−N π bonding and N lone-pair orbitals, respectively. However, HOMO-2, HOMO-3, and HOMO-4 (cf. Figure 1 of the Supporting Information) of CF_3CN reveal major contributions from the lone-pair orbitals of F atom and are closely spaced in energy. This results in the highly overlapping nature of the second photoelectron band of CF_3CN.

As discussed above the first band in the photoelectron spectrum of CF_3CN (cf. Figure 6) describes the vibronic structure of the $\tilde{X}-\tilde{A}$ coupled electronic states of CF_3CN^+. Low-energy conical intersections between the $\tilde{X}-\tilde{A}$ states are obtained along the symmetric vibrational mode of C−N stretching type. Although such conical intersections are located very near to the equilibrium geometries of these states for CF_3CN^+ (cf. panel a of Figure 1), they are located far away from the equilibrium geometries of these states for CH_3CN^+.[33] The JT interactions are weak in the $\tilde{X}$ state, in both CH_3CN^+ and CF_3CN^+. However, the $\tilde{X}-\tilde{A}$ PJT coupling is far stronger in CF_3CN^+, particularly along ν_8, compared to that in CH_3CN^+.[33] The harmonic frequency of this mode also reduces by a factor of 2 in CF_3CN^+. In summary, the far stronger PJT coupling leads to the highly diffuse vibronic structure of the first photoelectron band of CF_3CN^+ when compared to the same band of CH_3CN^+.[33]

Although He I and He II experimental results for the first band of CF_3CN^+ (cf. panel a of Figure 6) reveal no differences in the spectral intensities, the latter for the second band reveal dramatic differences. This bears the signature of ionization from MOs localized mainly on the CF_3 group, and this band appears well within the fingerprint region (15.0−17.5 eV) of CF_3 ionization.[34,35] The JT interactions in the $\tilde{D}$ electronic state have been shown to be much stronger than in the $\tilde{X}$ state. In addition, the PJT couplings between $\tilde{A}-\tilde{D}$ (through ν_6), $\tilde{B}-\tilde{D}$ (through ν_5, ν_6, and ν_7) and $\tilde{C}-\tilde{D}$ (through ν_5, ν_6, and ν_7) electronic states contribute substantially to the observed highly diffuse structure of this vibronic band.

VIII. Nonadiabatic Transitions: Time-Dependent Dynamics

In order to examine nonadiabatic transitions in the $\tilde{X}-\tilde{A}-\tilde{B}-\tilde{C}-\tilde{D}$ coupled electronic manifold and nonadiabatic decay of electronically excited states of CF_3CN^+, we recorded the time-dependence of the diabatic electronic populations for an initial transition to each of the above electronic states separately. The results are shown in Figure 7a−e. In panel a, the population dynamics is shown for an initial transition of the WP to one of the two JT split components of the $\tilde{X}$ state. The decay and growth of population of these components and the growth of the $\tilde{A}$ state population can be seen from the diagram. The population of the $\tilde{B}-\tilde{C}-\tilde{D}$ electronic states shows only minor variations in this case. It is therefore clear that the electronic nonadiabatic dynamics in this situation is predominantly governed by the JT coupling within the $\tilde{X}$ state and its PJT coupling with the $\tilde{A}$ state. The PJT conical intersections with the other electronic states occur at higher energies and remain inaccessible to the WP in this case. The initial decay of the population of the $\tilde{X}$ state relates to a decay rate of ~52 fs. It can be seen from panel a that the WP mostly undergoes nonadiabatic transitions back and forth between the two JT split components of the $\tilde{X}$ state. This is because the minimum of the $\tilde{X}-\tilde{A}$ conical intersections occurs ~0.43 eV above the minimum of the JT conical intersections within the $\tilde{X}$ state.

The population dynamics changes dramatically when the WP is initially prepared on the $\tilde{A}$ state, as shown in panel b. The $\tilde{X}-\tilde{A}$ PJT conical intersections are readily accessible to the WP packet in this case, and therefore, the population of the $\tilde{A}$ state decays at the much faster rate of ~22 fs. It can be seen that the decay of the $\tilde{A}$ state population mainly ("only") contributes to the growth of the population of the two components of the $\tilde{X}$ state. This reflects that the coupling of the $\tilde{A}$ state with $\tilde{B}$, $\tilde{C}$, and $\tilde{D}$ electronic states is not very significant (cf. Table 4).

The nonadiabatic transition dynamics of the WP initially prepared on the $\tilde{B}$ and $\tilde{C}$ states are shown in panels c and d,

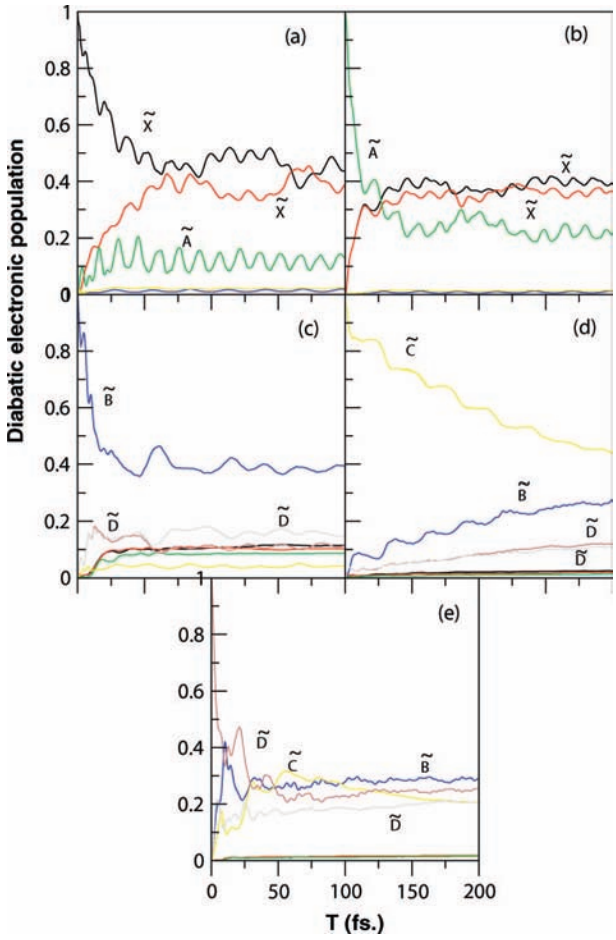

Figure 7. Time-dependence of diabatic electronic populations in the $\tilde{X}-\tilde{A}-\tilde{B}-\tilde{C}-\tilde{D}$ coupled states nuclear dynamics of CF_3CN^+. The results obtained by initially locating the WP on one component of the JT split $\tilde{X}$ state, $\tilde{A}$ state, $\tilde{B}$ state, and $\tilde{C}$ state and one component of the JT split $\tilde{D}$ state are shown in panels a−e, respectively.

respectively. In these cases, the transitions take place primarily within the $\tilde{B}-\tilde{C}-\tilde{D}$ electronic states only. The states within the $\tilde{X}-\tilde{A}$ electronic manifold mostly remain unpopulated during the dynamics. The decay rates of the $\tilde{B}$ and $\tilde{C}$ electronic states are estimated to be ∼32 and ∼125 fs, respectively, and are slower compared to that of the $\tilde{A}$ state.

Finally, the electronic population dynamics for an initial transition of the WP to one component of the JT split $\tilde{D}$ state is shown in panel e. It can be seen that the $\tilde{D}$ state decays at a much faster rate, ∼21 fs, compared to the $\tilde{X}$ state. This is due to the relatively stronger JT coupling within the $\tilde{D}$ state and also to the energetically close locations of the JT and $\tilde{B}-\tilde{D}$ and $\tilde{C}-\tilde{D}$PJT conical intersections. Only minor population transfer takes place to the $\tilde{X}-\tilde{A}$ coupled electronic manifold in this case also.

IX. Summary and Outlook

A detailed theoretical account of the multimode JT and PJT interactions in the five lowest electronic states of CF_3CN^+ have been presented here to elucidate highly complex vibronic structure of the first two photoelectron bands of CF_3CN. Extensive ab initio electronic structure calculations are performed to develop a vibronic coupling model (eqs 3–6e), and first-principles calculations are carried out both via time-independent and time-dependent quantal methods to simulate the nonadiabatic nuclear motion on the coupled manifold of these electronic states. The theoretical results are found to be in good accord with the available experimental results.

TABLE 5: PJT Coupling Parameters (in eV) of the Vibronic Hamiltonian of Eq 3

mode	$\lambda_i^{X,A}$	$\lambda_i^{X,B}$	$\lambda_i^{X,C}$	$\lambda_i^{A,D}$	$\lambda_i^{B,D}$	$\lambda_i^{C,D}$
ν_5	0.0203	0.0050	0.0020	0.0100	0.1570	0.0798
ν_6	0.0500	0.0400	0.0400	0.0636	0.0572	0.0496
ν_7	0.0500	0.0040	0.0800	0.0090	0.0639	0.0239
ν_8	0.1250	0.2500	0.2800	0.0070	0.0030	0.0070

The vibronic Hamiltonian is constructed in a diabatic electronic basis, including the JT coupling within the degenerate $\tilde{X}$ and $\tilde{D}$ electronic states and the PJT couplings of these JT split states with the nondegenerate $\tilde{A}$, $\tilde{B}$, and $\tilde{C}$ electronic states of CF_3CN^+. The coupling parameters of the vibronic Hamiltonian are determined by calculating the adiabatic PESs of the $\tilde{X}^2E$, $\tilde{A}^2A_1$, $\tilde{B}^2A_2$, $\tilde{C}^2A_1$, and $\tilde{D}^2E$ electronic states along each of the twelve vibrational modes.

The vibronic energy level structure of these electronic states of CF_3CN^+ are systematically examined at various level of theoretical approximations calculated by the time-independent matrix diagonalization approach. The final theoretical simulations using the full Hamiltonian of eqs 3–6e can only be carried out by propagating WPs by employing the MCTDH algorithm.[17–20] A careful examination of various theoretical results enabled us to arrive at the following conclusions. The symmetric vibrational modes ν_1 and ν_2 are crucial and are strongly excited. Whereas the former leads to low-energy crossings of the $\tilde{X}-\tilde{A}$ electronic states, the latter and ν_4 are both important for the low-energy crossings of $\tilde{B}-\tilde{C}-\tilde{D}$ electronic states. The JT effects in the $\tilde{X}$ electronic states is far weaker compared to that in the $\tilde{D}$ state. The JT stabilization energy of $\sim 4.6 \times 10^{-3}$ and ∼0.48 eV are estimated, respectively, for these electronic states. The JT and PJT interactions of the $\tilde{X}-\tilde{A}$ electronic states mostly contribute to the overall vibronic structure of the first photoelectron band. The PJT coupling due to ν_8 vibrational mode is found to be the strongest, and the vibrational modes ν_2, ν_7, and ν_8 are found to make the progressions in this band. Energetically close-lying $\tilde{B}-\tilde{C}-\tilde{D}$ electronic states are found to be responsible for the highly overlapping structure of the second photoelectron band. The relatively stronger JT coupling within the $\tilde{D}$ electronic state and appreciable PJT coupling due to ν_5 and ν_6 vibrational modes among these electronic states contributes to the diffuse vibronic structure of this band. The vibrational modes ν_2, ν_4, ν_5, and ν_7 form the major progressions in this band.

Acknowledgment. This study is in part supported by a research grant from the Department of Science and Technology, New Delhi (Grant no. DST/SF/04/2006). T.M. acknowledges the Council of Scientific and Industrial Research, New Delhi, for a Doctoral Fellowship. The use of computational facilities provided by the Center for Modeling Simulation and Design of the University of Hyderabad is gratefully acknowledged.

Supporting Information Available: This material is available free of charge via the Internet at http://pubs.acs.org.

References and Notes

(1) Born, M.; Oppenheimer, R. *Ann. Physik (Leipzig)* **1927**, *84*, 457.

(2) *Conical Intersections: Electronic Structure, Dynamics and Spectroscopy*; Domcke, W., Yarkony, D. R., Köppel, H. Eds.; World Scientific: Singapore, 2004.

(3) Köppel, H.; Domcke, W.; Cederbaum, L. S. *Adv. Chem. Phys.* **1984**, *57*, 59.

(4) (a) *Faraday Dicuss.* **2004**, *127*. (b) Conical intersections in photochemistry, spectroscopy and chemical dynamics. *Chem. Phys.* **2000**, *259*, 121−337.

(5) (a) Worth, G. A.; Cederbaum, L. S. *Annu. Rev. Phys. Chem.* **2004**, *55*, 127. (b) Mahapatra, S. *Int. Rev. Phys. Chem.* **2004**, *23*, 483.

(6) Jahn, H. A.; Teller, E. *Proc. R. Soc. London, Ser. A* **1937**, *161*, 220.

(7) (a) Öpik, U.; Pryce, M. H. L. *Proc. R. Soc London, Ser. A* **1957**, *238*, 425. (b) Longuet-Higgins, H. C.; Öpik, U.; Pryce, M. H. L.; Sack, R. A. *Proc. R. Soc. A.* **1958**, *244*, 1. (c) Longuet-Higgins, H. C. *Adv. Spectrosc.* **1961**, *2*, 429.

(8) Englman, R. *The Jahn-Teller Effect in Molecules and Crystals*; Wiley: New York, 1972.

(9) Bersuker, I. B.; Polinger, V. Z. *Vibronic Interactions in molecules and crystals*; Springer-Verlag: Berlin, 1989.

(10) (a) Teller, E. *J. Phys. Chem.* **1937**, *41*, 109. (b) Herzberg, G.; Longuet-Higgins, H. C. *Discuss Faraday Soc.* **1963**, *35*, 77. (c) Carrington, T. *Discuss. Faraday Soc.* **1972**, *53*, 27. (d) Yarkony, D. R. *Acc. Chem. Res.* **1998**, *31*, 511. (e) Bernardi, F.; Olivucci, M.; Robb, M. A. *Chem. Soc. Rev.* **1996**, *25*, 321.

(11) The Role of Degenerate States in Chemistry. In *Adv. Chem. Phys.*; Baer, M., Billing, G. D. Eds.; Wiley: Hoboken, 2002; Vol. 124.

(12) Bock, H.; Dammel, R.; and Lentz, D. *Inorg. Chem.* **1984**, *23*, 1535.

(13) (a) Perrin, M. H.; Gouterman, M. *J. Chem. Phys.* **1967**, *46*, 1019. (b) van der Waals, J. H.; Berghuis, A. M. D.; deGroot, M. S. *Mol. Phys.* **1967**, *13*, 301.

(14) Zgierski, M. Z.; Pawlikowski, M. *J. Chem. Phys.* **1979**, *70*, 3444.

(15) Köppel, H.; Cederbaum, L. S.; Domcke, W. *J. Chem. Phys.* **1988**, *89*, 2023.

(16) Holland, D. M. P.; Karlsson, L. *J. Electron Spectrosc. Relat. Phenom.* **2006**, *150*, 47.

(17) Worth, G. A.; Beck, M. H.; Jäckle, Meyer, H.-D. *The MCTDH Package*, University of Heidelberg: Germany, 2002; Version 8.3. See http://www.pci.uni-heidelberg.de/tc/usr/mctdh/.

(18) Meyer, H.-D.; Manthe, U.; Cederbaum, L. S. *Chem. Phys. Lett.* **1990**, *165*, 73.

(19) Manthe, U.; Meyer, H.-D.; Cederbaum, L. S. *J. Chem. Phys.* **1992**, *97*, 3199.

(20) Beck, M. H.; Jäckle, A.; Worth, G. A.; Meyer, H.-D. *Phys. Rep.* **2000**, *324*, 1.

(21) Frisch, M. J.; Trucks, G. W.; Schlegel, H. B.; Scuseria, G. E.; Robb, M. A.; Cheeseman, J. R.; Montgomery, J. A., Jr.; Vreven, T.; Kudin, K. N.; Burant, J. C.; Millam, J. M.; Iyengar, S. S.; Tomasi, J.; Barone, V.; Mennucci, B.; Cossi, M.; Scalmani, G.; Rega, N.; Petersson, G. A.; Nakatsuji, H.; Hada, M.; Ehara, M.; Toyota, K.; Fukuda, R.; Hasegawa, J.; Ishida, M.; Nakajima, T.; Honda, Y.; Kitao, O.; Nakai, H.; Klene, M.; Li, X.; Knox, J. E.; Hratchian, H. P.; Cross, J. B.; Bakken, V.; Adamo, C.; Jaramillo, J.; Gomperts, R.; Stratmann, R. E.; Yazyev, O.; Austin, A. J.; Cammi, R.; Pomelli, C.; Ochterski, J. W.; Ayala, P. Y.; Morokuma, K.; Voth, G. A.; Salvador, P.; Dannenberg, J. J.; Zakrzewski, V. G.; Dapprich, S.; Daniels, A. D.; Strain, M. C.; Farkas, O.; Malick, D. K.; Rabuck, A. D.; Raghavachari, K.; Foresman, J. B.; Ortiz, J. V.; Cui, Q.; Baboul, A. G.; Clifford, S.; Cioslowski, J.; Stefanov, B. B.; Liu, G.; Liashenko, A.; Piskorz, P.; Komaromi, I.; Martin, R. L.; Fox, D. J.; Keith, T.; Al-Laham, M. A.; Peng, C. Y.; Nanayakkara, A.; Challacombe, M.; Gill, P. M. W.; Johnson, B.; Chen, W.; Wong, M. W.; Gonzalez, C.; Pople, J. A. *Gaussian 03*, revision B.05; Gaussian, Inc.: Wallingford, CT, 2004.

(22) Shimizu, Y.; Ueda, K.; Chiba, H.; Okunishi, M.; Ohmori, K.; Sato, Y.; Suzuki, I. H.; Ibuki, T.; Okada, K. *Chem. Phys.* **1999**, *244*, 439.

(23) Åsbrnk, L.; Svensson, A.; Von Niesson, W.; Bieri, G. *J. Electron Spectrosc. Relat. Phenom.* **1981**, *24*, 293.

(24) Shimanouchi, T. Tables of molecular vibrational frequencies, consolidated volume I NSRDS NBS-39. Seehttp://srdata.nist.gov/cccbdb/.

(25) Wilson, E. B., Jr.; Decius, J. C.; Cross, P. C. *Molecular vibrations*; McGraw-Hill: New York, 1955.

(26) (a) Lichten, W. *Phys. Rev.* **1967**, *164*, 131. (b) Smith, F. T. *Phys. Rev.* **1969**, *179*, 111. (c) O'Malley, T. F. *Adv. At. Mol. Phys.* **1971**, *7*, 223. (d) Pacher, T.; Cederbaum, L. S.; Köppel, H. *Adv. Chem. Phys.* **1993**, *84*, 293.

(27) Domcke, W.; Köppel, H.; Cederbaum, L. S. *Mol. Phys.* **1981**, *43*, 851.

(28) Faraji, S.; Köppel, H.; Eisfeld, W.; Mahapatra, S. *Chem. Phys.* **2008**, *347*, 110.

(29) Cederbaum, L. S. *J. Phys. B* **1975**, *8*, 290.

(30) Cullum, J.; Willoughby, R. *Lanczos Algorithms for Large Symmetric Eigenvalue Problems*; Birkhäuser: Boston, 1985; Vols. *I*−*II*.

(31) Köppel, H.; Domcke, W. In *Encyclopedia of Computational Chemistry*; Schleyer, P. V. R. Ed.; Wiley: New York, 1998; p 3166.

(32) (a) Engel, V. *Chem. Phys. Lett.* **1992**, *189*, 76. (b) Manthe, U.; Meyer, H.-D.; Cederbaum, L. S. *J. Chem. Phys.* **1992**, *97*, 9062.

(33) Ghanta, S.; Mahapatra, S. *Chem. Phys.* **2008**, *347*, 97.

(34) Cvitas, T.; Güsten, H.; Klasinc, L.; Novak, I.; Vancik, H. *Z. Naturforsch.* **1977**, *1528*, 32a.

(35) Cvitas, T.; Novak, I.; Klasinc, L. *Int. J. Quan. Chem.* **1982**, *737*, 21.

JP801138A